A Low-RCS Wideband Antenna Based on Share-Structure of FSA and ME-Dipole

Youquan Wen, Sai-Wai Wong, Huawei Lin, Chunlin Ji, Ruopeng Liu, and Yejun He

***Abstract*—A wideband integrated antenna is proposed with the realization of radiation and dual-polarized absorption in the same frequency band. The novelty of the proposed integrated structure lies in the share-aperture of the frequency-selective absorber and magnetoelectric dipole, which remain mutually independent and have orthogonal operating characteristics. In the share-structure, each array element can be selectively connected to an excitation port or a resistor loading (50 Ω) to reuse the antenna port impedance for receiving and absorbing copolarized waves. While the cross-polarized waves are reflected by antenna ground and absorbed by mounted resistors on the symmetric patches at the top layer of the antenna array. Consequently, the proposed antenna exhibits both wideband radiation and dual-polarized absorption simultaneously with a low profile ($0.22\lambda_0$). Finally, a prototype 2×2 antenna array is fabricated and measured, demonstrating an impedance bandwidth of 92.7% for $|S_{11}| < -10$ dB from 2.2 to 6 GHz. Moreover, the proposed antenna has 10 dB RCS reduction bandwidth of 100% (2–6 GHz) for *x*- and *y*-polarized normally incident waves.**

***Index Terms*—Frequency-selective absorber (FSA), radar cross section (RCS), wideband antenna.**

I. Introduction

RECENTLY, the stealth performance of communication equipment has been crucial in military applications related to detection and communication [1]. Low radar cross section (RCS) antennas have gained significant traction in integrated sensing and communication by effectively reducing the target signature of military communication equipment under radar detection [2]. A common approach for RCS reduction of antenna involves the use of metasurface to scatter the incident electromagnetic (EM) wave to lower the EM radiation energy in particular directions or absorb EM energy [3], [4].

For the first category, a variety of checkerboard arrays such as artificial magnetic conductors (AMC) [5], polarization converters [6], [7] and coding metasurfaces [8] find extensive applications in RCS reduction. For another, frequency-selective absorbers (FSAs) have been proposed in the literature, also offering the advantage of reducing the RCS [9], [10]. FSAs are placed above the antenna, which allows the passage of in-band waves and absorbs out-of-band waves. However, achieving low in-band RCS of the antenna remains a challenge, as it involves a significant tradeoff between radiation and absorption characteristics. In [11], [12], [13], [14], and [15], these common methods such as using polarization rotation reflective surfaces to isolate col-polarized and cross-polarized waves or using diodes to switch the radiation and absorption states. However, aforementioned structures use separated circuits and separated layers, which leads to a higher profile. Those FSAs usually exhibit a narrow frequency response and filtering characteristics, which impose constraints on the antenna bandwidth or radiation efficiency. Therefore, it is of great significance to design a low-profile wideband antenna that possesses the advantages of both wideband operation and low RCS using the FSA technique.

In recent years, there has been a tendency to focus excessively on improving FSA designs to achieve in-band low RCS for antennas, which has led to a fixed mindset. In contrast, the inherent characteristics and design aspects of the antenna itself are usually overlooked or underestimated. Magnetoelectric dipole (ME-dipole) consists of the horizontal patch (operates as an electric dipole) and vertical quarter-wave shorted metalized vias (operates as a magnetic dipole) [16]. For ME-dipoles, the ideal height is typically chosen to be a quarter of electrical length ($\lambda_l/4$) for optimal matching performance and good radiation pattern [17]. As for the design of FSA, the thickness is also commonly corresponds to a quarter wavelength ($\lambda_f/4$) of the resonant frequency, enabling the FSA to achieve a maximum absorption of specific frequencies of EM waves. Therefore, the integrated structure of FSA and ME-dipole can achieve wideband radiation for communication and wideband absorption for low RCS performance simultaneously.

In this letter, a wideband integrated antenna is proposed with a dual function of radiation and absorption in the same frequency band. The shared structure of the FSA and ME-dipole is adopted to achieve the share aperture, resulting in a compact and lower-profile design when compared with reported works that involve stacking separate circuits and layers. Moreover, both FSA and antenna have wideband performance with both functions more than fractional bandwidth (FBW) of 92.7% and overlapping the same wideband frequency in this proposed work.

II. Geometry and Analysis of Antenna Element

Fig. 1 illustrates the schematic model of an integrated array antenna. The proposed antenna acts as a share-structure base on ME-dipole and FSA, which consists of a patch-layer loaded with resistors, vertical metalized pillars and a slot layer. For

Manuscript received 25 February 2024; accepted 28 March 2024. Date of publication 1 April 2024; date of current version 4 December 2024. This work was supported in part by the National Natural Science Foundation of China under Grant 62171289 and Grant 62071306, and in part by the National Key Research and Development Program of China under Grant 2023YFE0107900. *(Corresponding author: Sai-Wai Wong.)*

Youquan Wen, Sai-Wai Wong, and Yejun He are with the State Key Laboratory of Radio Frequency Heterogeneous Integration, Guangdong Engineering Research Center of Base Station Antennas, Shenzhen Key Laboratory of Antennas and Propagation, College of Electronics and Information Engineering, Shenzhen University, Shenzhen 518060, China (e-mail: wongsaiwai@ieee.org).

Huawei Lin is with the Faculty of Science and Technology, University of Macau, Taipa 519000, Macau.

Chunlin Ji and Ruopeng Liu are with the Kuang-Chi Institute of Advanced Technology, Shenzhen 518000, China.

Digital Object Identifier 10.1109/LAWP.2024.3383853

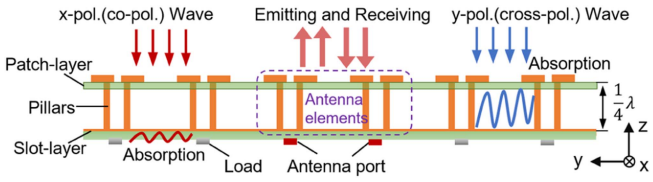

Fig. 1. Schematic model of integrated array antenna (Section view of $x = 0$).

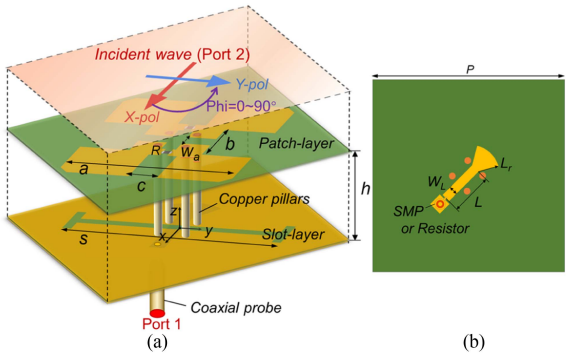

Fig. 2. Unit cell of the proposed integrated antenna. (a) 3-D view of the proposed integrated antenna and FSA, (b) bottom view of the slot-layer. (Structure parameters: $P = 45.2$, $a = 32$, $b = 11$, $c = 7$, $w_a = 2.5$, $s = 32$, $W_L = 2.4$, $L = 13.3$, $L_r = 6.5$, $h = 16$, all in mm; $R = 225\ \Omega$).

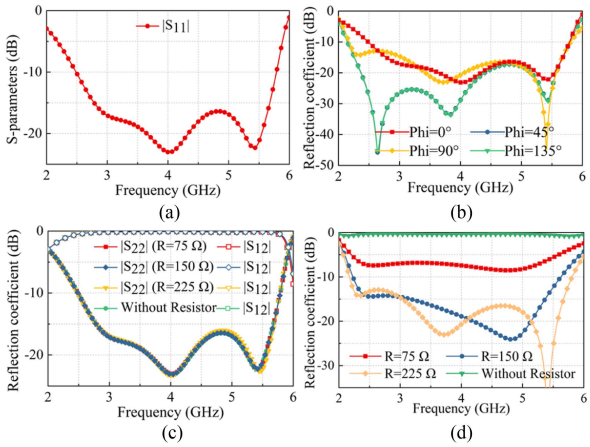

Fig. 3. Simulated results of the unit cell of the proposed integrated antenna. (a) $|S_{11}|$. (b) Reflection coefficients for different Phi incident waves. (c) Reflection coefficients for an x-polarized wave with different resistances. (d) Reflection coefficients for a y-polarized wave with different resistances.

radiation, the proposed arrays are excited by aperture-coupled feeding on center elements of slot layer. Each array element can be selectively connected to an excitation port or a resistor loading (50 Ω) to re-use the antenna port impedance for receiving. For incident waves, the integrated structure can be regarded as a frequency-selective absorber. The copolarized wave can be received through the slot and be absorbed by resistors of 50 Ω on the rest elements of the slot-layer. While the cross-polarized waves are reflected by antenna ground and absorbed by mounted resistors on the symmetric patches at the top layer of the antenna array. Thus, both the copolarized and cross-polarized waves are absorbed by the integrated structure. Consequently, the proposed antenna exhibits both wideband radiation and low in-band radar cross section.

Fig. 2 illustrates the geometry of the unit cell of the integrated antenna. As shown in Fig. 2(a), the integrated antenna consists of the patch layer, vertical copper pillars, and slot-layer. The patch-layer comprises four symmetrical patches that are etched on a F4BM substrate with a permittivity of 2.65 and thickness of 0.3 mm, which act as E-dipoles. Two pairs of symmetrical patches are designed as a Minkowski island for size reduction [18]. Two resistors are connected to the two pairs of patches, which parallel to the x-axis. The length of each patch is about a quarter wavelength ($\lambda_f/4$) with respect to the lower resonant frequency of the antenna, where λ_f is the corresponding wavelength. The vertical copper pillars are mounted between the patch-layer and the feed-layer through metal vias, which work as M-dipoles. The height of vertical copper pillars is denoted as h. The slot-layer incorporates features such as an I-shaped slot and a fan-shaped microstrip line aimed at achieving miniaturization and broadband matching. The slot is positioned at the center of the four vertical copper pillars and parallel to the y-axis. As shown in Fig. 2(b), the bottom surface of the slot-layer etches a fan-shaped microstrip line with the other side fed by a 50 Ω coaxial probe, and the thickness of slot-layer is 1 mm.

Fig. 3 shows simulated results of the proposed integrated antenna at the boundary conditions of the unit cell. When Port 1 acts as excitation, it can be seen in Fig. 3(a) that the antenna achieves an impedance-matching bandwidth of 2.5–5.8 GHz (FBW = 79.5%) and transmit to free space. Fig. 3(b) shows the reflection coefficient when Port 2 acts as a different polarized incident wave from free space. In this condition, Port 1 acts as a resistor loading of 50 Ω; thus, the reflection coefficient ($|S_{22}|$) can represent absorption. When Phi = 0 (x-polarized wave), it can be seen that the reflection coefficient is the same result as in Fig. 3(a). According to the antenna reciprocity, it also indicates that the x-polarized incident wave (copolarized wave) has entered the slot-layer and been absorbed by Port 1 [19]. When Phi = 90 (y-polarized wave, or cross-polarized incident wave), the reflection coefficient is less than −10 dB over the frequency range of 2.2–5.8 GHz (FBW = 90%). Moreover, the reflection coefficients for different Phi incident waves are stable. It can be indicated that the proposed antenna has wideband absorption for any polarized incident wave. Fig. 3(c) and (d), respectively, shows the reflection coefficients for x-polarization and y-polarization with different resistances of R. It can be seen that the result for x-polarization is not affected by the value of surface resistors, incident wave smoothly is absorbed by Port 1. For y-polarization, when no resistor is added, the incident wave is fully reflected. It illustrates that the y-polarized waves can be reflected by the slot-layer (acts as ground) and then be absorbed by patch-layer loaded with resistors. When $R = 225\ \Omega$, the results reach maximum absorption bandwidth.

The surface current at 4 GHz for y-polarized wave is presented in Fig. 4(b). The surface current is concentrated at the edges of the patches (parallel to the y-axis), while the current at the outer edges (parallel to the x-axis) is very weak. It can be observed that the location of the current concentration is precisely different from the distribution in Fig. 4(a). Therefore, it can be inferred that the radiation characteristics of the antenna and the absorption properties of the FSA remain mutually independent and orthogonal. In consequence, it verifies the feasibility of the share-aperture based on ME-dipole and the FSA, preliminarily.

The equivalent circuit model is regarded as an efficient way to analyze the reflection behavior for the incident waves with two different polarizations. For the x-polarization, Fig. 5(a) presents

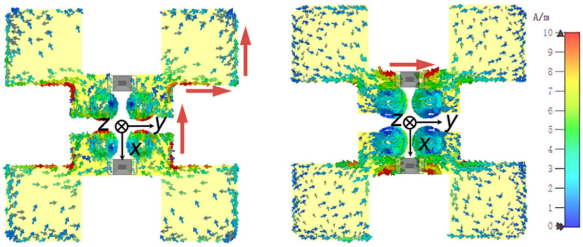

Fig. 4. Current distribution of the proposed integrated antenna at 4 GHz for different polarization. (a) *x*-polarization. (b) *y*-polarization.

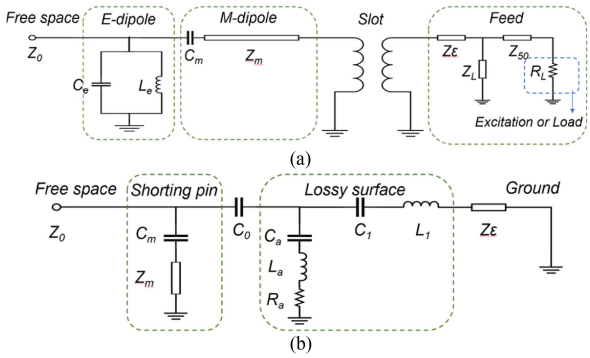

Fig. 5. Equivalent circuit model for (a) *x*-polarization; and (b) *y*-polarization.

the equivalent circuit model of the structure, which works as the ME-dipole. As the model, the impedance of the free space and the dielectric substrate can be equivalent to Z_0 and Z_ε. The patch-layer can be seen as an LC parallel circuit, where the inductor L_e denotes the patches, and the capacitor C_e denotes the gap between the adjacent patches. In this model, the resonant frequency f is determined by the following formula [13]:

$$f = \frac{1}{2\pi\sqrt{L_e C_e}} \tag{1}$$

and the characteristic impedance of Z_e can be determined by the formula [23]

$$Z_e = \sqrt{\frac{L_e}{C_e}}. \tag{2}$$

By adjusting the values of capacitance and inductance, specific resonant frequencies can be achieved, enabling the antenna to have higher radiation efficiency and optimal impedance matching at operating frequency. The capacitor C_m denotes the discontinuous coupling structure between the patches and the pillar. The transmission line with the impedance of Z_m denotes the vertical pillars between the patch-layer and the feed-layer, which is determined by the formula [16]

$$Z_m = \frac{1}{2} Z_d = \frac{60}{\sqrt{\varepsilon_r}} \operatorname{arcosh}\left(\frac{\mathrm{D_r}}{2\mathrm{r_0}}\right) \tag{3}$$

where ε_r is the relative permittivity, D_r is the center spacing of two adjacent copper pillars, and r_0 is the diameter of the copper pillar. The slot on the front side of the feed-layer is equivalent to a transformer. Last, the feeding network on the backside of the feed-layer can be denoted as a microstrip transmission line Z_L connected in parallel with a matching load R_L. Fig. 5(b) presents the equivalent circuit model for the *y*-polarization. For

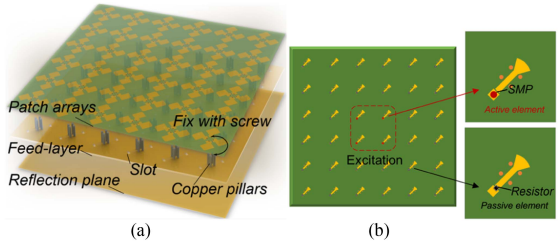

Fig. 6. Geometry of integrated antenna arrays. (a) Schematic view of assembly structure. (b) Bottom view of feed-layer.

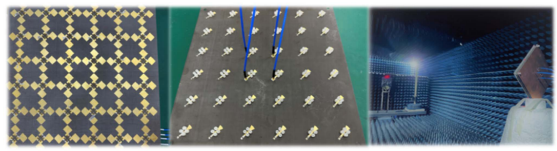

Fig. 7. Prototype of integrated antenna arrays. (a) Top view of patch arrays. (b) Feed-layer of 2 × 2 excited arrays. (c) Photograph of the measurement setup.

the *y*-polarized waves, it can be regarded as the FSA mentioned previously [20]. The patch-layer can be equivalent to a lossy surface instead of an E-dipole. In the lossy surface, the inside edges of the patches connected resistors form an RLC series circuit, with the other end grounded. The outer boundary of the patches is equivalent to a capacitor C_1 in series with an inductor L_1. Besides, the capacitor C_m and the transmission line Z_m can be considered as the M-dipole, which is in series with the ground. Based on these correlations between circuit and size parameters, it has obtained optimized parameters for the proposed shared-structure as shown in Fig. 2.

III. Antenna Array and Experimental Results

A. Integrated Structure of Antenna Arrays

Fig. 6(a) presents the geometry of the integrated structure of antenna arrays. The structure is composed of 6 × 6 unit cells with checkerboard arrays. The overall size of the structure is $3.73\lambda_0 \times 3.73\lambda_0 \times 0.36\lambda_0$ (λ_0 is the wavelength at the center frequency of 4 GHz in free space). The patch arrays and copper pillars are fixed with screws, which work as ME-dipole arrays. As shown in Fig. 6(b), 2 × 2 antenna elements in the center are excited by the aperture-coupled feeding with 50 Ω port impedance. The rest of the unexcited feedings are terminated with resistors loading of 50 Ω. The prototype of the integrated structure is fabricated and presented in Fig. 7. Furthermore, this integrated structure can excite an arbitrary number of antenna elements. Besides, the addition of the reflection copper plate below the feed-layer serves to reduce backward radiation and diffraction which did not affect the absorber performance. To verify this feasibility, the feed-layer with 2 × 2 excited antenna elements is designed to be driven by four coaxial ports in Fig. 7(b). It is noteworthy that, a 2 × 2 antenna array is only an example. The number of antenna array elements can be arbitrary chosen, e.g., 4 × 4 antenna array elements as well. It can be adopted to increase the gain by connecting antenna elements to the feeding port through a power divider network.

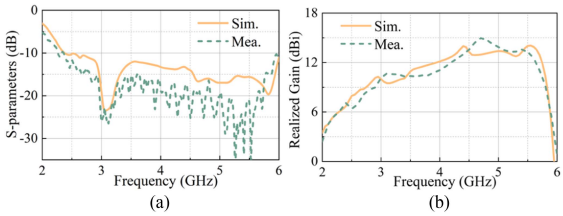

Fig. 8. (a) Simulated and measured S-parameters of 2 × 2 excited arrays. (b) Simulated and measured gains of 2 × 2 excited arrays.

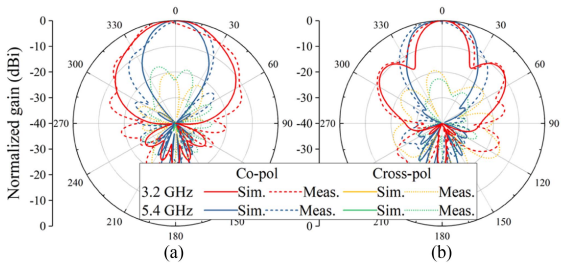

Fig. 9. Simulated and measured radiation patterns of 2 × 2 excited arrays at (a) *xoz*-plane; and (b) *yoz*-plane.

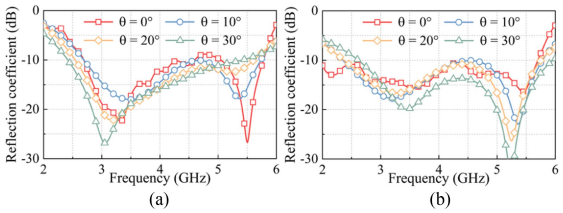

Fig. 10. Measured reflection coefficient of the proposed integrated antenna under different oblique incidences: (a) x- and (b) y-polarization.

B. Radiation Performance

For the 2 × 2 excited arrays, Fig. 8(a) illustrates the simulated and measured S-parameters. The simulated impedance bandwidth is 89.2%, with $|S_{11}| < -10$ dB from 2.3 to 6 GHz. The measured impedance bandwidth is about 92.7%, with $|S_{11}| < -10$ dB from 2.2 to 6 GHz. A good agreement has been obtained between the simulated and the measured results. Fig. 8(b) presents the realized gain of the 22 excited arrays, which shows the consistent trend of measured results and simulated ones. Some deviations may arise from dielectric losses, installation tolerance, as well as environment uncertainties. Fig. 9 gives the radiation patterns at 3.2 and 5.4 GHz, respectively. The radiation patterns of the antenna array remain relatively stable across two frequency bands. The cross-polarization levels of measurements are below −20 dB in both the *xoz*-plane and *yoz*-plane. By comparing measured and simulated results, it can be observed a good agreement between them.

C. Scattering Performance

To verify the absorption of the proposed antenna, the reflection coefficients under different oblique incidences are measured by the arch method [24]. In Fig. 10, it can be noticed that the prototype shows a stable reflection coefficient when the oblique incidence is less than 30° under both x- and y-polarization (TM and TE modes) [21], [25]. Furthermore, in order to show the effect of the proposed antenna on RCS reduction, both the monostatic RCS of the proposed antenna are investigated and compared with the reference antenna. Fig. 7(c) illustrates the measurement setup in an anechoic chamber. The fabricated antenna prototype is vertically positioned on a foam platform and terminated with a matched load. Differing from the proposed antenna, the reference antenna lacks the installation of ME-dipole arrays and resistors on the feed-layer. Fig. 11 respectively depicts the monostatic RCS results. For the x-polarization, the proposed antenna achieves an RCS reduction of 10 dB from 2.8 to 6 GHz (FBW = 72.7%). For the y-polarization, it achieves a low RCS band from 2 to 6 GHz (FBW = 100%). It indicates that a wideband RCS reduction is obtained for both of x-polarized and y-polarized incident waves. Finally, to better understand the attractive advantages of the proposed integrated device, a comparative study with other reported low-RCS antennas is tabulated in Table I. The comparison with other reported works has validated the effectiveness of the proposed structure in the design of low-RCS antennas. The proposed antenna has the widest impedance FBW of 92.7% and a comparable low profile, as well as a wide RCS reduction FBW of 100%.

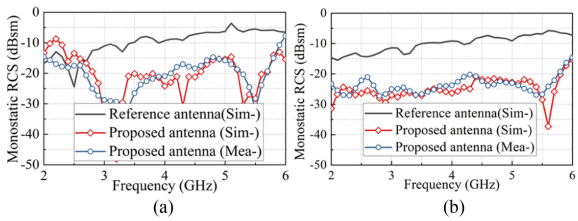

Fig. 11. Simulated and measured monostatic RCS of the proposed integrated antenna: (a) x- and (b) y-polarization.

TABLE I
COMPARISONS OF PARAMETERS AMONG LOW-RCS ANTENNAS

Ref.	Structure	Impedance, FBW	Size($\lambda_0\times\lambda_0\times\lambda_0$)	RCS reduction, FBW
[11]	HMS+antenna	9.5-10.2 GHz, 7.1%	2.2×2.2×0.8	6-18 GHz (>5 dB), 100%
[14]	Reconfigurable FSA+antenna	8.15-8.5 GHz, 3.6%	1.88×2.08×0.2	4.02-13.82 GHz (>10 dB), 101%
[15]	FSA+CP antenna	4.5-5.7 GHz, 23.5%	1.89×1.89×0.23	2.5-5.7 GHz (>10 dB), 78%
[22]	ATFSS+F-P cavity antenna	7.3-7.7 GHz, 5.3%	2×1.75×0.8	4-7.2 GHz (>5 dB), 57.1%
This work	FSA&ME-dipole	**2.2-6 GHz, 92.7%**	3.73×3.73×0.22	2-6 GHz (>10dB), 100%

IV. CONCLUSION

In this letter, the low RCS wideband antenna based on the share-structure of FSA and ME-dipole has been proposed and fabricated. The integrated structure appears to be well-designed for both antenna radiation and FSA absorption simultaneously. The performances of an antenna are measured and analyzed. The results demonstrate that the proposed antenna has broadband impedance bandwidth and RCS reduction when it compares with reported works. Overall, the proposed work can address the challenges of wireless communication and in-band RCS reduction effectively, and the design of share-structure is verified to be a promising approach in low-profile and wideband integrated devices.

REFERENCES

[1] E. F. Knott, J. F. Shaeffer, and M. T. Tuley, *Radar Cross Section*. Stevenage, U.K.: SciTech, 2004.

[2] L. Gan, W. Jiang, Q. Chen, X. Li, Z. Zhou, and S. Gong, "Method to estimate antenna mode radar cross section of large-scale array antennas," *IEEE Trans. Antennas Propag.*, vol. 69, no. 10, pp. 7029–7034, Oct. 2021.

[3] Y. Azizi et al., "Wideband RCS reduction by single-layer phase gradient modulated surface," *Sensors*, vol. 22, no. 19, 2022, Art. no. 7108.

[4] X. Xu et al., "Deterministic approach to achieve broadband polarization-independent diffusive scatterings based on metasurfaces," *IEEE Access*, vol. 5, pp. 1691–1702, 2017.

[5] Y. F. Cheng, L. Yang, X. Zhong, C. Liao, and X. Ding, "Analysis and design of wideband low-RCS Fabry–Perot antennas with reduced profile," *IEEE Trans. Antennas Propag.*, vol. 70, no. 9, pp. 7934–7943, Sep. 2022, doi: 10.1109/TAP.2022.3177488.

[6] M. K. T. Al-Nuaimi, S.-L. Zhu, W. G. Whittow, G.-L. Huang, R.-S. Chen, and Q. Shao, "Design of polarization-insensitive and angularly stable metasurfaces with symmetric cubic phase distribution for broadband RCS reduction," *IEEE Trans. Antennas Propag.*, vol. 71, no. 1, pp. 1069–1074, Jan. 2024.

[7] M. K. T. Al-Nuaimi, Y. He, and W. Hong, "Scattered EM-wave shaping using combination of cross-polarization conversion and reflection phase cancellation," *IEEE Antennas Wireless Propag. Lett.*, vol. 18, no. 2, pp. 318–322, Feb. 2018.

[8] M. K. T. Al-Nuaimi et al., "Coding engineered reflector for wide-band RCS reduction under wide angle of incidence," *IEEE Trans. Antennas Propag.*, vol. 70, no. 10, pp. 9947–9952, Oct. 2022.

[9] Y. He et al., "Design of an adjustable polarization-independent and wide-band electromagnetic absorber," *J. Appl. Phys.*, vol. 119, no. 10, Mar. 2016, Art. no. 105103.

[10] Y. Pang et al., "Wideband RCS reduction metasurface with a transmission window," *IEEE Trans. Antennas Propag.*, vol. 68, no. 10, pp. 7079–7087, Oct. 2020.

[11] Y. Liu, Y. Jia, W. Zhang, and F. Li, "Wideband RCS reduction of a slot array antenna using a hybrid metasurface," *IEEE Trans. Antennas Propag.*, vol. 68, no. 5, pp. 3644–3652, May 2020.

[12] M. Li, Z. Yi, Y. Luo, B. Muneer, and Q. Zhu, "A novel integrated switchable absorber and radiator," *IEEE Trans. Antennas Propag.*, vol. 64, no. 3, pp. 944–952, Mar. 2016.

[13] J. Sun, Q. Cao, Y. Li, and H. Li, "Functional reconfigurable integrated structure of circularly polarized antenna and FSS absorber," *IEEE Trans. Antennas Propag.*, vol. 69, no. 11, pp. 7260–7268, Nov. 2021.

[14] J. Sun, Q. Cao, M. Pan, and L. Zhu, "A broadband multilayer absorber with switchable function of radiation," *IEEE Trans. Antennas Propag.*, vol. 70, no. 8, pp. 6841–6849, Aug. 2022.

[15] Y. Han, L. Zhu, Y. Bo, W. Che, and B. Li, "Novel low-RCS circularly polarized antenna arrays via frequency-selective absorber," *IEEE Trans. Antennas Propag.*, vol. 68, no. 1, pp. 287–296, Jan. 2020.

[16] H. Lin, Y. Li, S.-W. Wong, K. W. Tam, B. Liu, and L. Zhu, "High-selectivity FA-FA-based frequency selective surfaces using magnetoelectronic dipole antennas," *IEEE Trans. Antennas Propag.*, vol. 70, no. 11, pp. 10669–10677, Nov. 2022.

[17] L. Ge and K. M. Luk, "A low-profile magneto-electric dipole antenna," *IEEE Trans. Antennas Propag.*, vol. 60, no. 4, pp. 1684–1689, 2012.

[18] S. Zheng, Y. Yin, J. Fan, X. Yang, B. Li, and W. Liu, "Analysis of miniature frequency selective surfaces based on fractal antenna–filter–antenna arrays," *IEEE Antennas Wireless Propag. Lett.*, vol. 11, pp. 240–243, 2012.

[19] M. S. Neiman, "The principle of reciprocity in antenna theory," *Proc. IRE*, vol. 31, no. 12, pp. 666–671, Dec. 1943.

[20] X. Q. Lin, P. Mei, P. C. Zhang, Z. Z. D. Chen, and Y. Fan, "Development of a resistor-loaded ultrawideband absorber with antenna reciprocity," *IEEE Trans. Antennas Propag.*, vol. 64, no. 11, pp. 4910–4913, Nov. 2016.

[21] Z. Ma, C. Jiang, W. Cao, J. Li, and X. Huang, "An ultrawideband and high-absorption circuit-analog absorber with incident angle-insensitive performance," *IEEE Trans. Antennas Propag.*, vol. 70, no. 10, pp. 9376–9384, Oct. 2022.

[22] W. Yu, Y. Yu, W. Wang, X. H. Zhang, and G. Q. Luo, "Low-RCS and gain-enhanced antenna using absorptive/transmissive frequency selective structure," *IEEE Trans. Antennas Propag.*, vol. 69, no. 11, pp. 7912–7917, Nov. 2021.

[23] S. Ghosh and K. V. Srivastava, "An equivalent circuit model of FSS-based metamaterial absorber using coupled line theory," *IEEE Antennas Wireless Propag. Lett.*, vol. 14, pp. 511–514, 2015.

[24] W. Hofmann, C. Bornkessel, A. Schwind, and M. A. Hein, "Challenges of RF absorber characterization: Comparison between RCS- and NRL-arch-methods," in *Proc. Int. Symp. Electromagn. Compat.-Europe*, 2019, pp. 370–375.

[25] K. Wang et al., "Broadband and broad-angle low-scattering metasurface based on hybrid optimization algorithm," *Sci. Rep.*, vol. 4, no. 1, 2014, Art. no. 5935.